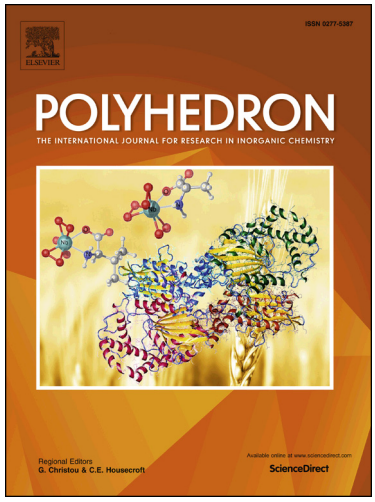

Synthesis, characterization, luminescent properties and biological activities of zinc complexes with bidentate azomethine Schiff-base ligands

A.S. Burlov, V.G. Vlasenko, Yu.V. Koshchienko, N.I. Makarova, A.A. Zubenko, Yu.D. Drobin, L.N. Fetisov, A.A. Kolodina, Ya.V. Zubavichus, A.L. Trigub, S.I. Levchenkov, D.A. Garnovskii

PII: S0277-5387(18)30430-3
DOI: https://doi.org/10.1016/j.poly.2018.07.034
Reference: POLY 13299

To appear in: *Polyhedron*

Received Date: 1 June 2018
Revised Date: 19 July 2018
Accepted Date: 21 July 2018

Please cite this article as: A.S. Burlov, V.G. Vlasenko, Yu.V. Koshchienko, N.I. Makarova, A.A. Zubenko, Yu.D. Drobin, L.N. Fetisov, A.A. Kolodina, Ya.V. Zubavichus, A.L. Trigub, S.I. Levchenkov, D.A. Garnovskii, Synthesis, characterization, luminescent properties and biological activities of zinc complexes with bidentate azomethine Schiff-base ligands, *Polyhedron* (2018), doi: https://doi.org/10.1016/j.poly.2018.07.034

Synthesis, characterization, luminescent properties and biological activities of zinc complexes with bidentate azomethine Schiff-base ligands

A. S. Burlov[a], V. G. Vlasenko[b,*], Yu. V. Koshchienko[a], N. I. Makarova[a], A. A. Zubenko[c], Yu. D. Drobin[c], L.N. Fetisov[c], A.A. Kolodina[a], Ya. V. Zubavichus[d], A. L. Trigub [d], S. I. Levchenkov[e], D. A. Garnovskii[e]

[a]*Institute of Physical and Organic Chemistry of Southern Federal University, Stachki ave. 194/2, Rostov-on-Don 344090, Russian Federation;*
e-mail: anatoly.burlov@yandex.ru
[b]*Institute of Physics of Southern Federal University, Stachki ave. 194, Rostov-on-Don 344090, Russian Federation*
[c]*North-Caucasian Zonal Scientific Research Veterinary Institute – Branch of the Federal State Budget Scientific Institution "Federal Rostov Agricultural Research Centre", Rostov highway, 0, Novocherkassk 346421, Russian Federation*
[d]*NRC Kurchatov Institute, 1 Acad. Kurchatov Sq., Moscow 123182, Russian Federation*
[e]*Southern Scientific Centre of Russian Academy of Sciences, Chekhova ave. 41, Rostov-on-Don 344006, Russian Federation*

Keywords: Azomethines, Zinc complexes, UV-Vis spectra, Photoluminescence, Biological activity

A B S T R A C T

A series of zinc complexes with a bidentate azomethine Schiff base ligands derived from 2-tosylaminobenzaldehyde, 2-hydroxy-, 2-hydroxy-5-methoxybenzaldehydes, 2-hydroxynaphthaldehyde and 3,4-dimethoxyphenylethylamine were synthesized by chemical and electrochemical methods. All compounds were characterized on the basis of C, H, N elemental analysis, FT-IR, ^{1}H NMR, UV-vis and photoluminescence studies.

[*]Corresponding author
E-mail address: v_vlasenko@rambler.ru

The local atomic structures of complexes were determined from analysis of EXAFS and XANES of Zn K-edges. The molecular structure of bis{2-[(E)-2-(3,4-dimethoxyphenyl)ethyliminomethyl]-4-methoxyphenol}zinc(II) was determined by X-ray single-crystal diffraction. The fluorescence spectra show that these complexes in DMSO solutions at room temperature emit bright blue and green luminescence at 428-497 nm. The assignment and the nature of the bands in experimental UV-vis spectra of complexes were analyzed using time-dependent (TD) DFT calculations. The azomethines and complexes of zinc have been screened for their antibacterial, protistocidal, and fungistatic activities against *Penicillium italicum*, *Colpoda steinii*, *Escherichia coli 078* and *Staphylococcus aureus P-209*, and the results are compared with the activity of sulfadimethoxine, toltrazuril and fundazol.

1. Introduction

Zinc(II) complexes of bi-, tri-, tetradentate azomethine ligands receive strong attention due to their various functional properties. They show antibacterial, antimicrobial [1, 2], and antitumor [3-9] activity. Many zinc complexes of azomethine ligands are effective luminophores emitting in the range of 400-450 nm and are in great demand as photo- and electroluminescent materials [10-20]. Such emitters are the main constituent of red-green-blue luminescent displays, as well as key luminescent components in the formation of white radiation by a combination of blue and orange colors [10].

The photo- and electroluminescent properties of zinc complexes of bidentate azomethine ligands derived from 2-hydroxybenzaldehyde have been studied by many authors [21-24]. The maxima of longwave absorption bands of these complexes are located in the 400-412 nm range, whereas that of photoluminescence at 450-550 nm. Quantum yields of PL in these zinc complexes are low: 0.007-0.0057 [11, 15, 22]. The substitution of the hydroxy group in the aldehyde fragment of bidentate azomethine ligands by the 2-tosylamino group results in formation of chelate zinc complexes with ZnN_4 coordination site and improvement of their thermal stability [12, 25-30]. Such synthetic available zinc complexes, which luminescent in the blue spectral region λ_{PL} =

428 – 433 nm with quantum luminescence yields φ = 0.23 – 0.37 and have melting points above 230 °C, were used as emitting materials for design of OLED devices by many authors [11, 14, 16, 29, 30].

Since there are much fewer compounds capable of emitting blue light than red and green, the expansion of the series of luminescence complexes in the 400-500 nm region is an important and urgent task.

Moreover, the presence of pharmacophore methoxy groups in the amine fragment and the sulfonamide group in the aldehyde fragment of the complexes can have a significant effect on their biological properties.

The present work is devoted to the synthesis of zinc complexes of bidentate azomethine ligands derived from 2-tosylaminobenzaldehyde, 2-hydroxy-, 2-hydroxy-5-methoxybenzaldehydes, 2-hydroxynaphthaldehyde and 3,4-dimethoxyphenylethylamine, and to the study of their structures, photoluminescence and biological properties.

2. Experimental

2.1. Materials required and general methods

All solvents, zinc acetate dihydrate CAS № 5970-45-6, 2-Hydroxybenzaldehyde CAS № 90-02-8, 2-Hydroxy-5-methoxybenzaldehyde CAS №: 672-13-9, 2-Hydroxy-1-naphthaldehyde CAS №708-06-5, 3,4-Dimethoxyphenylethylamine CAS № 120-20-7 were purchased from Alfa Aesar and used as received. 2-(N-Tozylamino)benzaldehyde has been synthesized using the reported procedure [31].

C, H, N elemental analyses were carried out on a Carlo Erba TCM 480 apparatus using sulfanilamide as a reference. The metal content was determined gravimetrically in the analytical laboratory of the Institute of Physical and Organic Chemistry (SFU, Rostov-on-Don, Russia). Melting points were measured on a Kofler table.

Infrared spectra were recorded on a Varian Excalibur-3100 FT-IR spectrophotometer for powders of compounds **1b-d** and **2a-d**.

^{1}H NMR spectra were measured on a Varian Unity-300 (300 MHz) spectrometer at ambient temperature in $CDCl_3$. The chemical shifts (δ) were referenced to residual solvent shifts in the respective deuterated solvents.

UV-Vis spectra were registered on «Varian Cary 100» spectrophotometer. Photoluminescent spectra were measured on a «Varian Cary Eclipse» fluorescence spectrophotometer. DMSO of the spectrally pure grade from Sigma-Aldrich was used as a solvent. All UV-Vis and fluorescence spectra were recorded using standard quartz cells with an optical path of 1 cm at room temperature at $c = 4.0 \times 10^{-5}$ M. Fluorescence quantum yield were determined by Parker-Reese technique [32] using 3-methoxybenzathrone in toluene ($\varphi = 0.1$, $\lambda_{ex} = 365$ nm) as a standard luminophor [33].

2.2. Synthesis of free ligands

*2.2.1. A general procedure for the synthesis of N-[2-[(E)-2-(3,4-dimethoxyphenyl)ethyliminomethyl]phenyl]-4-methylbenzenesulfonamide (**1a**), 2-[(E)-2-(3,4-dimethoxyphenyl)ethyliminomethyl]phenol (**1b**), 2-[(E)-2-(3,4-dimethoxyphenyl)ethyliminomethyl]-4-methoxyphenol (**1c**), and 1-[(E)-2-(3,4-dimethoxyphenyl)ethyliminomethyl]naphthalen-2-ol (**1d**).*

Solution of 0.36 g (2 mmol) of 3,4-dimethoxyphenylethylamine in 10 ml of ethanol was added to a solution of 0.55 g (2 mmol) of 2-N-tosylaminobenzaldehyde for **1a**, 0.24 g (2 mmol) of 2-hydroxybenzaldehyde for **1b**, 0.30 g (2 mmol) of 2-hydroxy-5-methoxybenzaldehyde for **1c**, 0.34 g (2 mmol) 2-hydroxy-1-naphthaldehyde for **1d** in 15 ml of ethyl alcohol. The mixture was refluxed for 2 h. After cooling azomethine precipitates were filtered off, washed with 5 ml of ethanol and recrystallized from ethanol.

*2.2.2. N-[2-[(E)-2-(3,4-Dimethoxyphenyl)ethyliminomethyl]phenyl]-4-methylbenzenesulfonamide (**1a**)*

Yellow crystals, m.p. = 110-111 °C. Yield 0.78 g, 89%. Anal. Calc. for $C_{24}H_{26}N_2O_4S$: C, 65.73; H, 5.98; N, 6.38. Found: C, 65.84; H, 6.01; N, 6.29 %. IR spectrum, selected bands, cm^{-1}: 3000-2833 ν(CH_2), 1633 ν(CH=N), 1328 $\nu_{as}(SO_2)$, 1153

ν_s (SO_2). ^{1}H NMR, δ (ppm): 2.35 (s, 3H, CH_3), 3.02 (t, 2H, ^{3}J=7.0 Hz, CH_2), 3.80 (s, 3H, OCH_3), 3.82-3.87 (m, 5H, OCH_3, CH_2), 6.74-6.82 (m, 3H, C_{Ar}-H), 6.96-7.01 (m, 1H, C_{Ar}-H), 7.14-7.29 (m, 4H, C_{Ar}-H), 7.60 (d, 1H, ^{3}J=8.4 Hz, C_{Ar}-H), 7.71 (d, 2H, ^{3}J=8.4 Hz, C_{Ar}-H), 8.09 (s, 1H, CH=N), 13.13 (s, 1H, NH).

*2.2.3. 2-[(E)-2-(3,4-Dimethoxyphenyl)ethyliminomethyl]phenol (**1b**)*

Yellow crystals, m.p. = 74-75 °C. Yield 0.51 g, 90%. Anal. Calc. for $C_{17}H_{19}NO_3$: C, 71.56; H, 6.71; N, 4.91. Found: C, 71.61; H, 6.68; N, 4.82 %. IR spectrum, selected bands, cm^{-1}: 2999-2836 ν(CH_2), 1633 ν(CH=N), 1260 ν(Ph-O). ^{1}H NMR, δ (ppm): 2.95 (t, 2H, ^{3}J=6.9 Hz, CH_2), 3.81 (s, 3H, OCH_3), 3.82 (s, 2H, CH_2), 3.85 (s, 3H, OCH_3), 6.71 (d, 1H, ^{4}J=1.5 Hz, C_{Ar}-H), 6.75 (dd, 1H, ^{3}J=8.1 Hz, ^{4}J=1.8 Hz, C_{Ar}-H), 6.80 (d, 1H, ^{3}J=8.1 Hz, C_{Ar}-H), 6.85 (t, 1H, ^{3}J=7.5 Hz, C_{Ar}-H), 6.95 (d, 1H, ^{3}J=8.4 Hz, C_{Ar}-H), 7.18 (d, 1H, ^{3}J=7.8 Hz, C_{Ar}-H), 7.31 (dd, 1H, ^{3}J=8.5 Hz, ^{4}J=1.5 Hz, C_{Ar}-H), 8.19 (s, 1H, CH=N), 13.52 (s, 1H, OH).

*2.2.4. 2-[(E)-2-(3,4-Dimethoxyphenyl)ethyliminomethyl]-4-methoxyphenol (**1c**)*

Yellow crystals, m.p. = 50-51 °C. Yield 0.54 g, 85%. Anal. Calc. for $C_{18}H_{21}NO_4$: C, 65.55; H, 6.71; N, 4.44. Found: C, 65.60; H, 6.69; N, 4.50 %. IR spectrum, selected bands, cm^{-1}: 3000-2842 ν(CH_2), 1638 ν(CH=N), 1256 ν(Ph-O). ^{1}H NMR, δ (ppm): 2.95 (t, 2H, ^{3}J=6,8 Hz, CH_2), 3.76 (s, 3H, OCH_3), 3.80 (s, 2H, CH_2), 3.81 (s, 3H, OCH_3), 3.85 (s, 3H, OCH_3), 6.69-6.81 (m, 4H, C_{Ar}-H), 6.90 (s, 2H, C_{Ar}-H), 8.15 (s, 1H, CH=N), 13.00 (s, 1H, OH).

*2.2.5. 1-[(E)-2-(3,4-Dimethoxyphenyl)ethyliminomethyl]naphthalen-2-ol (**1d**)*

Yellow crystals, m.p. = 101-102 °C. Yield 0.46 g, 68%. Anal. Calc. for $C_{21}H_{21}NO_3$: C, 75.20; H, 6.31; N, 4.18. Found: C, 75.31; H, 6.28; N, 4.29 %. IR spectrum, selected bands, cm^{-1}: 3000-2845 ν(CH_2), 1630 ν(CH=N), 1286 ν(Ph-O). ^{1}H NMR, δ (ppm): 2.99 (t, 2H, ^{3}J=6.8 Hz, CH_2), 3.81-3.83 (m, 8H, 2OCH_3, CH_2), 6.73-6.83 (m, 3H, C_{Ar}-H), 6.92 (d, 1H, ^{3}J=9.3 Hz, C_{Ar}-H), 7.21 (t, 1H, ^{3}J=7.5 Hz, C_{Ar}-H),

7.38 (t, 1H, ^{3}J=7,8 Hz, C_{Ar}-H), 7.59 (d, 1H, ^{3}J=7.5 Hz, C_{Ar}-H), 7.66 (d, 1H, ^{4}J=2.1 Hz, C_{Ar}-H), 7.69 (s, 1H, CH=N), 8.48 (d, 1H, ^{3}J=8,4 Hz, C_{Ar}-H), 14.51 (s, 1H, OH).

2.3. Synthesis of complexes

2.3.1. The general procedure for the preparation of complexes **2a-d**

Chemical synthesis (CS). Solution of 1 mmol (0.22 g) of zinc acetate dihydrate in 5 ml of ethanol was added to a solution of 1 mmol of the corresponding azomethine ligand (0.43 g of azomethine **1a**, 0.29 g of azomethine **1b**, 0.32 g of azomethine **1c**, 0.34 g of azomethine **1d**) in 20 ml of ethanol. The mixture was refluxed for 2 h. The precipitates of complexes **2a-d** were filtered off, washed with ethanol (5 ml) and recrystallized from dichloromethane-ethanol (1:2) mixture.

Electrochemical synthesis (ES). A solution of 1 mmol of the corresponding ligand (0.43 g of azomethine **1a**, 0.29 g of azomethine **1b**, 0.32 g of azomethine **1c**, 0.34 g of azomethine **1d**) in 20 ml of acetonitrile was placed in an electrochemical cell with a platinum cathode and zinc anode and 0.01 g of $[Et_4N]ClO_4$ was added as electrolyte.

ES were performed during 1 h at 40 mA and 20 V at r. t. The precipitates of complexes were filtered off and crystallized from a chloroform-ethanol (1:2) mixture.

Electrochemical cell:

Cathode (Pt): $2LH+2e\rightarrow 2L^{-2}+H_2$

Anode (Zn): $Zn^{0}-2e\rightarrow Zn^{2+}$

Solution: $2L^{-2}+Zn^{2+}\rightarrow ZnL_2$

*2.3.2. Bis{N-[2-[(E)-2-(3,4-dimethoxyphenyl)ethyliminomethyl]phenyl]-4-methylbenzenesulfonamide}zinc(II) (**2a**)*

Colorless crystals, m.p. = 247-248 °C. Yield 0.42 g, 90%. Anal. Calc. for $C_{48}H_{50}N_4O_8S_2Zn$: C, 61.42; H, 5.44; N, 6.01; Zn, 7.12 %. Found: (CS) C, 61.55; H, 5.50; N, 6.15; Zn, 7.32 %. (ES) C, 61.38; H, 5.38; N, 6.14; Zn, 7.20 %. IR spectrum, selected bands, cm^{-1}: 3051-2836 ν(CH_2), 1630 ν(CH=N), 1258 $\nu_{as}(SO_2)$, 1132 $\nu_{s}(SO_2)$. ^{1}H NMR, δ (ppm): 2.28 (s, 6H, CH_3), 2.63-2.73 (m, 2H, CH_2), 2.93-3.03 (m, 2H, CH_2), 3.57-3.66 (m, 2H, CH_2), 3.69 (s, 6H, OCH_3), 3.81 (s, 6H, OCH_3), 4.45-4.54 (m, 2H,

CH_2), 6.51-6.57 (m, 4H, C_{Ar}-H), 6.69 (d, 2H, ^3J=8.1 Hz, C_{Ar}-H), 6.81 (t, 2H, ^3J=7.4 Hz, C_{Ar}-H), 7.08 (d, 4H, ^3J=8.1 Hz, C_{Ar}-H), 7.17-7.22 (m, 4H, C_{Ar}-H), 7.53 (d, 2H, ^3J=9.0 Hz, C_{Ar}-H), 8.08 (d, 4H, ^3J=8.1 Hz, C_{Ar}-H), 8.18 (s, 2H, CH=N).

*2.3.3. Bis{2-[(E)-2-(3,4-dimethoxyphenyl)ethyliminomethyl]phenol} zinc(II) (**2b**)*

Yellow crystals, m.p. = 194-195 °C. Yield 0.28 g, 89%. Anal. Calc. for $C_{34}H_{36}N_2O_6Zn$: C, 64.48; H, 5.63; N, 4.32.; Zn, 10.48 %. Found: (CS) C, 64.62; H, 5.58; N, 5.54; Zn, 10.32 %. (ES) C, 64.58; H, 5.70; N, 4.28; Zn, 10.54 %. IR spectrum, selected bands, cm^{-1}: 2985-2835 ν(CH_2), 1613 ν(CH=N), 1325 ν(Ph-O). ^{1}H NMR, δ (ppm): 2.87 (t, 4H, ^3J=7.5 Hz, CH_2), 3.68 (s, 6H, OCH_3), 3.72 (d, 4H, ^3J=7.5 Hz, CH_2), 3.81 (s, 6H, OCH_3), 6.55-6.56 (m, 2H, C_{Ar}-H), 6.60 (d, 4H, ^3J=8.1 Hz, C_{Ar}-H), 6.71 (d, 2H, ^3J=8.1 Hz, C_{Ar}-H), 6.90 (d, 2H, ^3J=8.7 Hz, C_{Ar}-H), 7.03 (dd, 2H, ^3J=7.8 Hz, ^4J=1.5 Hz, C_{Ar}-H), 7.31 (t, 2H, ^3J=7.8 Hz, C_{Ar}-H), 7.99 (s, 2H, CH=N).

*2.3.4. Bis{2-[(E)-2-(3,4-dimethoxyphenyl)ethyliminomethyl]-4-methoxyphenol}zinc(II) (**2c**)*

Yellow crystals, m.p. = 200-201 °C. Yield 0.23 g, 65%. Anal. Calc. for $C_{36}H_{40}N_2O_8Zn$: C, 62.30; H, 5.81; N, 4.04.; Zn, 9.42 %. Found: (CS) C, 62.42; H, 5.78; N, 4.12; Zn, 9.54 %. (ES) C, 62.15; H, 5.90; N, 3.98; Zn, 9.37 %. IR spectrum, selected bands, cm^{-1}: 3000-2842 ν(CH_2), 1623 ν(CH=N), 1302 ν(Ph-O). ^{1}H NMR, δ (ppm): 2.86 (t, 4H, ^3J=7.5 Hz, CH_2), 3.68-3.70 (m, 10H, OCH_3, CH_2), 3.74 (s, 6H, OCH_3), 3.82 (s, 6H, OCH_3), 6.49 (d, 2H, ^4J=3.0 Hz, C_{Ar}-H), 6.55 (d, 2H, ^4J=1.8 Hz, C_{Ar}-H), 6.61 (dd, 2H, ^3J=6.9 Hz, ^4J=1.8 Hz, C_{Ar}-H), 6.72 (d, 2H, ^3J=8.1 Hz, C_{Ar}-H), 6.86 (d, 2H, ^3J=9.0 Hz, C_{Ar}-H), 7.01 (dd, 2H, ^3J=9.0 Hz, ^4J=3.2 Hz, C_{Ar}-H), 7.96(s, 2H, CH=N).

*2.3.5. Bis{1-[(E)-2-(3,4-dimethoxyphenyl)ethyliminomethyl]naphthalen-2-ol}zinc(II) (**2d**)*

Yellow crystals, m.p. = 204-205 °C. Yield 0.24 g, 65%. Anal. Calc. for $C_{42}H_{40}N_2O_6Zn$: C, 68.71; H, 5.49; N, 3.82.; Zn, 8.91 %. Found: (CS) C, 68.65; H, 5.52; N, 3.90; Zn, 9.10 %. (ES) C, 68.80; H, 5.42; N, 3.74; Zn, 9.15 %. IR spectrum, selected

bands, cm^{-1}: 3054-2893 ν(CH_2), 1607 ν(CH=N), 1341 ν(Ph-O). ^{1}H NMR, δ (ppm): 2.91 (t, 4H, ^{3}J=7.2 Hz, CH_2), 3.54 (s, 6H, OCH_3), 3.75 (s, 6H, OCH_3), 3.83 (t, 4H, ^{3}J=7.0 Hz, CH_2), 6.53 (s, 2H, C_{Ar}-H), 6.62-6.68 (m, 4H, C_{Ar}-H), 7.10 (d, 2H, ^{3}J=9.3 Hz, C_{Ar}-H), 7.22 (d, 2H, ^{3}J=7.5 Hz, C_{Ar}-H), 7.41 (t, 2H, ^{3}J=7.5 Hz, C_{Ar}-H), 7.66 (d, 2H, ^{3}J=7.8 Hz, C_{Ar}-H), 7.74-7.77 (m, 4H, C_{Ar}-H), 8.94(s, 2H, CH=N).

2.4. X-ray Crystallography Analysis of zinc complex **2c**.

Diffraction data for **2c** were collected at 173(2) K on a Bruker APEX2 platform-CCD X-ray diffractometer system equipped with a graphite monochromatized Mo *K*α X-ray source with a wavelength of λ = 0.71073 Å, 50 kV/40 mA power. Detailed description of X-ray crystallographic experiment is given in Supplementary Materials. Crystallographic data for **2c** are summarized in Table 1, the fractional atomic coordinates and isotropic or equivalent isotropic displacement parameters are given in Tables S1-S4 Supplementary Materials. All calculations were carried out using the SHELX-97 program [34].

Supplementary data CCDC 1846537 contains the supplementary crystallographic data for **2c**. These data can be obtained free of charge via http://www.ccdc.cam.ac.uk/conts/retrieving.html, or from the Cambridge Crystallographic Data Centre, 12 Union Road, Cambridge CB2 1EZ, UK; fax: (+44) 1223-336-033; or e-mail: deposit@ccdc.cam.ac.uk.

Table 1

Crystal data and structure refinement parameters for complex **2c**.

Compound	**2c**
Empirical formula	$C_{36}H_{40}N_2O_8Zn$
M	694.07
Crystal size, mm	0.32 × 0.22 × 0.05
T, K	173
Crystal system	Monoclinic
Space group	*C*2
a, Å	18.6407 (9)

b, Å	8.3884 (4)
c, Å	12.9283 (6)
β , °	125.500 (1)
V, Å^3	1645.77 (14)
Z	2
$\rho_{calc.}$, g/cm^3	1.401
μ, mm^{-1}	0.80
F(000)	728
θ Range (°)	2.2–31.2
Reflections collected	9969
Unique reflections	4876
Reflections with $I > 2\sigma(I)$	4656
Index ranges	h = -26→26
	k = -11→11
	l = -18→18
R_1 ($I > 2\sigma(I)$)	0.026
wR_2 (all reflections)	0.056
GOF	0.99
Residual electron density, $\Delta\rho_{max}$/ $\Delta\rho_{min}$, *e*Å^{-3}	0.61/-0.30

2.5. X-ray absorption spectroscopy

The Zn *K*-edge EXAFS spectra for the complexes **2a-d** were recorded at the "Structural Materials Science" beamline of the Kurchatov Synchrotron Radiation Source (Moscow, Russia) [35] with the storage ring operating at electron energy of 2.5 GeV and current of 80−100 mA. A Si(111) channel-cut monochromator was used for the energy selection. All data were measured in the transmission mode. Sample thicknesses corresponded to an absorption jump Δμx=0.5–1.0.

EXAFS data (χ_{exp}(k)) were analyzed using the IFEFFIT data analysis package [36]. EXAFS data reduction used standard procedures for the pre-edge subtraction and spline background removal. The radial pair distribution functions around the Zn ions were obtained by the Fourier transformation (FT) of the k^3-weighted absorption function χ_{exp}(k) range of photoelectron wave numbers k = 2.4–13.0 Å^{-1}. Structural parameters including interatomic distances (R_i), coordination numbers (N_i) and distance

RMS deviations due to the thermal motion and disorder-induced static deviations of atomic positions, also known as Debye–Waller factors (σ^2) were found by non-linear fitting of the theoretical spectra against the experimental ones.

$$\chi(k) = S_0{}^2 \sum_{i=1}^{n} \frac{N_i}{R_i{}^2} \frac{F_i(k)}{k} e^{-\frac{2R_i}{\lambda(k)}} e^{-2\sigma_i{}^2 k^2} \sin(2kR_i + \Psi_i(k)), \quad (1)$$

The experimental data were simulated using theoretical photoelectron mean-free-path (λ), photoelectron backscattering amplitude $F_i(k)$ and phase functions (formula 1) calculated using the FEFF7 program [37]. The amplitude reduction factor due to extrinsic losses $S_0{}^2$ and the edge energy shift E_0 were calibrated by fitting EXAFS data for spectra of reference compounds with known crystal structures. The amplitude reductions factors $S_0{}^2$ were found to be equal to 0.9 in all cases.

The accuracy of the fits was estimated by the standard mean-square deviation criterion (formula 2) (Q-factor),

$$Q^2 = \frac{\sum_{i=1}^{m} w(k_i)\left[k_i \chi_{\exp}(k_i) - k_i \chi_{th}(k_i)\right]^2}{\sum_{i=1}^{m} w(k_i)\left[k_i \chi_{\exp}(k_i)\right]^2} \quad (2)$$

where $w(k_i)$ is a weighting function, m is the number of experimental points.

2.6. Quantum-chemical calculations

The GAUSSIAN-03 program package [38] was used for DFT calculations. Ground-state geometry of isolated molecules of the complexes under study was optimized using the Becke's three-parameter exchange functional [39], Lee–Yang–Parr correlation functional (B3LYP) [40] and standard split-valence polarized 6-31G(d) basis set [41, 42]. The absence of imaginary frequencies in the normal mode analysis ensured optimized geometry to be the true energy minimum, not a transition state.

The simulation of UV-vis absorption spectra for these complexes was performed within the Time-Dependent Density Functional Theory (TD-DFT) formalism using the optimized geometry subject to solvent effects as predicted by the standard polarizable continuum model (PCM) [43]. The lowest 50 singlet-to-singlet spin-allowed excitation

states were taken into account for the calculations of the electronic absorption spectra of complexes **2a-d.**

2.7. Antimicrobial activity assay

Antimicrobial properties of azomethines **1a-d** and complexes **2a-d** were studied by means of two-fold serial dilutions in a liquid nutrient medium [44, 45]. Suspensions of bacterial cultures (2 mL) with a concentration of $5.0 \cdot 10^5$ microbial cells per mL were mixed with equal amount of test substance solutions at variable concentrations in special vials (which gave rise to a nominal two-fold decrease in the bacteria concentration to $2.5 \cdot 10^5$ per mL). Vials were kept in an incubator for 18 h at 37 °C. In parallel, vials containing nutrient medium and bacteria at a concentration of $2.5 \cdot 10^5$ per mL and only nutrient medium without bacteria were incubated under identical conditions as positive control and negative control probes, respectively. Standard strains of bacteria *Staphylococcus aureus P-209* and *Escherichia coli 078* (field isolates from the collection of the Rostov regional veterinary laboratory) were used for the antimicrobial activity tests. Activity of the azomethines and zinc complexes was compared with that of a commercial antibiotic sulfadimethoxine (chemically pure grade).

2.8. Antiprotozoal activity assay

Antiprotozoal activity was studied against infusoria *Colpoda steinii* (field isolate from the collection of the laboratory of parasitology of the North-Caucasian Zonal Scientific-Research Veterinary Institute, Russia) using a method described elsewhere [46]. The tests were carried out in a 96-well microplate typically used for the enzyme-linked immunosorbent assays (ELISA), 12 wells of the first row were used. A 1:1 mixture of boiled tap and sterile distilled water was used as a medium. Initially the substance being tested was dissolved in distilled water. Serial dilutions of the test solutions were prepared as follows:

Solution No.1: 5 mg of the substance under study was dissolved in 50 μL of 70% aqueous DMSO under stirring, then 5 mL of distilled water was carefully added to give

an apparent concentration of the probe 1000 µg/mL, 150 µL of the prepared solution was placed into the well No.1 of the microplate.

Solutions No.2-12: 150 µL of 1:1 mixture of boiled tap and sterile distilled water was placed into the wells No.2-12 of the microplate using an automated 8-channel pipette. Then 150 µL of the solution No.1 was placed into the well No.2 under stirring. After complete mixing an aliquot of 150 µL of solution No.2 was placed into the well No.3. A similar procedure was applied to all further wells. In order to provide identical volumes of solutions in all the wells, 150 µL of the solution was removed from the last well No.12. Aliquots of the *Colpoda steinii* protozoa culture suspended in water preliminary incubated for 3 days (30 µL) were added to all wells in such a way that no less than 10-15 active infusoria were distinctly visible in the field-of-view of an optical microscope. The microplate was covered with a lid and left at room temperature (20-22 °C) for 18-20 h.

Test results were controlled as follows: 30 µL of content of each well one-by-one starting from the well No.12 was transferred onto a clean glass slide and examined under an optical microscope at a magnification of 10×15 to check for the presence of living protozoa. The minimum protistocidal concentration of a substance under study corresponded to the first well encountered with no living infusoria. In a similar way, the following control solutions were tested:

- blank medium (boiled water + distilled water) – 5 wells;
- DMSO (50 µL of 70% DMSO + 5 mL of distilled water serially diluted exactly as in the case of the tested substances) – 12 wells;
-commercial antiprotozoal agent toltrazuril (2.5% solution serially diluted similarly to the tested substances).

2.9. Fungistatic activity assay

Antifungal activity of the compounds was determined by the agar-diffusion method according to the guideline [47] for fungi culture *Penicillium italicum Wehmer* (1894) (field isolate, from the collection of micromycetes of the laboratory of mycotoxicology of the North-Caucasian Zonal Scientific Research Veterinary Institute,

Russia). A commercial fungicide fundazol was used for comparison. An aqueous solution of the test compounds or fundazol for comparison were placed on a disc of filter paper (ND-PMP-1 Paster Central Research Institute of Epidemiology and Microbiology) in an amount of 15 μg per disc with a diameter of 8 mm.

3. Results and discussion

3.1. Synthesis and spectroscopic properties of azomethines as free ligands and their derived zinc complexes

The azomethine compounds **1a-d** (HL) were obtained by condensation of 2-N-tosylaminobenzaldehyde (for **1a**), 2-hydroxybenzaldehyde (for **1b**), 2-hydroxy-5-methoxybenzaldehyde (for **1c**), 2-hydroxy-1-naphthalaldehyde (for **1d**) and 3,4-dimethoxyphenylethylamine in ethanol solutions (Scheme).

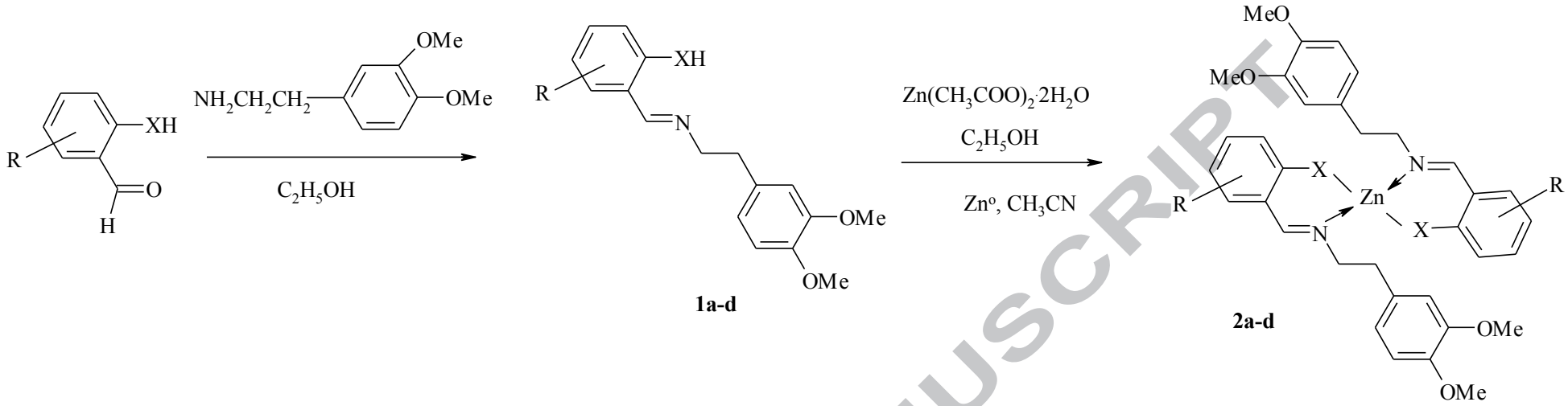

a (R=H, X= NSO_2 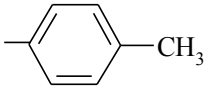 CH_3); **b** (R=H, X=O); **c** (R= 5-OCH_3, X= O);

d (R= 5,6-cyclo-C_4H_4, X=O)

Scheme. Synthesis of the azomethines **1a-d** and zinc complexes **2a-d**

Zinc complexes **2a-d** were obtained by two methods: chemical (refluxing of azomethine compounds **1a-d** with zinc acetate dihydrate at a molar ratio of 2:1 in ethanol) and electrochemical (by anodic dissolution of zinc in acetonitrile azomethine solution **1a-d**).

The structures of azomethines **1a-d** and zinc complexes **2a-d** were determined by means of IR, ^{1}H NMR spectroscopy and elemental analysis.

All azomethine compounds **1a-d** are crystalline substances. In the IR spectra of compounds **1a-d**, absorption bands are observed at the 1630-1638 cm^{-1} ν(CH=N), in the case of **1a** there are also absorption bands at 1328 cm^{-1} $\nu_{as}(SO_2)$ and 1153 cm^{-1} $\nu_s(SO_2)$, whereas in the cases of **1b-d** at 1260, 1256, 1286 cm^{-1} ν(Ph-O), respectively. Due to the presence of strong intramolecular hydrogen bond XH...N in the azomethines **1a-d**, in their IR spectra the ν(NH, OH) absorption bands in the region 3000-3500 cm^{-1} are not observed. In the ^{1}H NMR spectra of these compounds, the proton signals of CH=N, NH and OH groups are registered at 7.69-8.19 (**1a-d**), 13.13 (**1a**) and 13.00-14.51 ppm (**1b-d**), respectively.

According to the elemental analysis data the zinc complexes possess ZnL_2 composition. In the IR spectrum of **2a**, the absorption bands of ν(CH=N) shift to lower frequencies by 3 cm^{-1}, whereas of $\nu_{as}(SO_2)$ and $\nu_s(SO_2)$ by 32 cm^{-1} and 20 cm^{-1}, respectively. In the IR spectra of **2b-d**, the ν(CH=N) absorption bands also redshift by 15-23 cm^{-1}, and the absorption bands ν(Ph-O) blueshift by 45-65 cm^{-1}. In the ^{1}H NMR spectra of **2a-d**, the proton signals of the NH and OH groups of azomethines **1a-d** disappear. The proton signals of the CH=N groups downfield by 0.9 (**2a**) and 1.25 ppm (**2d**) or upfield by 0.2 (**2b**) and 0.19 ppm (**2c**).

3.2. The X-ray absorption spectroscopy

X-ray absorption spectroscopy (XAS), including extended X-ray absorption fine structure (EXAFS) and X-ray absorption near-edge structure (XANES) analysis, has been carried out at the Zn K edge of the zinc coordination compounds **2a-d**. From analysis of the Zn XANES spectra, the local electronic structure of Zn atoms is described. Fig. 1a displays the background subtracted and normalized Zn K edge XANES spectra and

their first derivatives of four complexes **2a-d**. The XANES spectra of Zn *K*-edges, indicating that the Zn atoms are predominantly present in a divalent oxidation state occupying the center of tetrahedral configuration. No 1s–3d transitions are expected due to the lack of empty d states in Zn^{2+} ions (d^{10}).

Analysis of EXAFS of Zn *K*-edges has been used to provide information about the quantitative characteristics of the local structure around zinc ions in complexes **2a-d**. The structural data for the complex **2c** determined by the X-ray crystallography were used as the starting model for all Zn(II) complexes in the EXAFS analysis.

From the Fourier transforms of the Zn K-edge k^3-weighted EXAFS spectra (Fig. 1b), major peak can be observed at 1.52-1.58 Å, corresponding to the Zn–N (**2a**) and Zn-O/N (**2b-d**) distances. Minor shells at > 2 Å are also observed, which give evidence for ligand coordination. The EXAFS fitting results of the first-neighbor feature show an average coordination number of 4 (Table 2) for the Zn-N or Zn-N/O shells in the samples, indicating that the zinc(II) ions have a tetrahedral coordination environment, which is in accordance to our findings from XANES.

The average distances Zn–N (2a), Zn-O/N (**2b-d**) and magnitudes of Debye-Waller factors for all complexes have typical values in similar zinc complexes with tetrahedral geometry about metal center [12, 48-50].

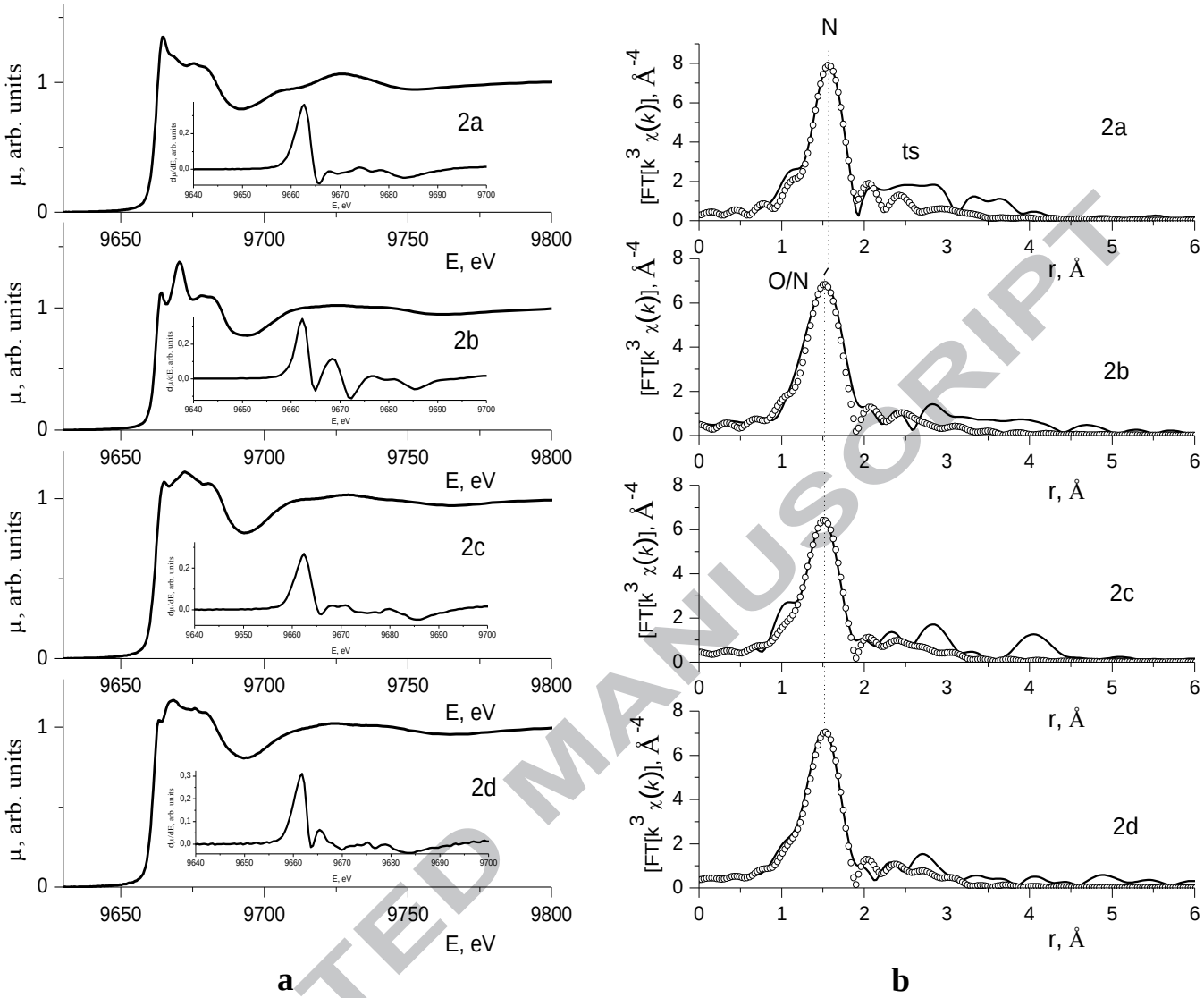

Fig. 1. Zn *K*-edge XANES spectra for the zinc complexes **2a-d** (a) represented as μ(E) and dμ/dE (insets) (a), MFT EXAFS $\chi(k)k^3$ for zinc complexes **2a-d**, experiment - solid line, best-fit theory - empty circles (b).

Table 2

Parameters of the local structure around zinc ions in complexes **2a-d**: coordination numbers (N), interatomic distances (R), and Debye-Waller factors (σ^2). Q is the integral fit quality factor.

Compound	N	R, Å	σ^2, Å^2	KC	Q, %
2a	4	2.00	0.0033	N	2.1

2b	2	1.92	0.0040	O	1.0
	2	2.02	0.0040	N	
2c	2	1.91	0.0041	O	2.6
	2	2.02	0.0041	N	
2d	2	1.91	0.0039	O	1.7
	2	2.01	0.0039	N	

EXAFS fitting: Δr= 1.0-2.0 Å

3.3. The X-ray diffraction

The molecular structure and atom numbering scheme of the complex **2c** are shown in Fig. 2. The molecule of **2c** has *C*2 symmetry. The Zn(II) center displays a distorted tetrahedral geometry with a N_2O_2 ligand environment. The azomethine ligands act as the bidentate chelating species and are coordinated to the central ion in *trans*-positions through deprotonated phenolic oxygen atoms O(1) and O(1a) and azomethinic nitrogen atoms N(1) and N(1a). The dihedral angle between the planes N(1)O(1)Zn(1) and N(1a)O(1a)Zn(1) is equal to 78.93º.

The six-membered chelate rings adopt a half-boat conformation, with the Zn atom deviating 0.274 Å from the plane formed by N(1)C(8)C(6)C(1)O(1) (the maximum mean-plane deviation for C(8) is 0.028 Å). As can be seen from data of selected bondlengths for **2c** (Fig.2), the agreement between EXAFS and crystallography was excellent for the major shells (distances underestimated by only 0.02 Å).

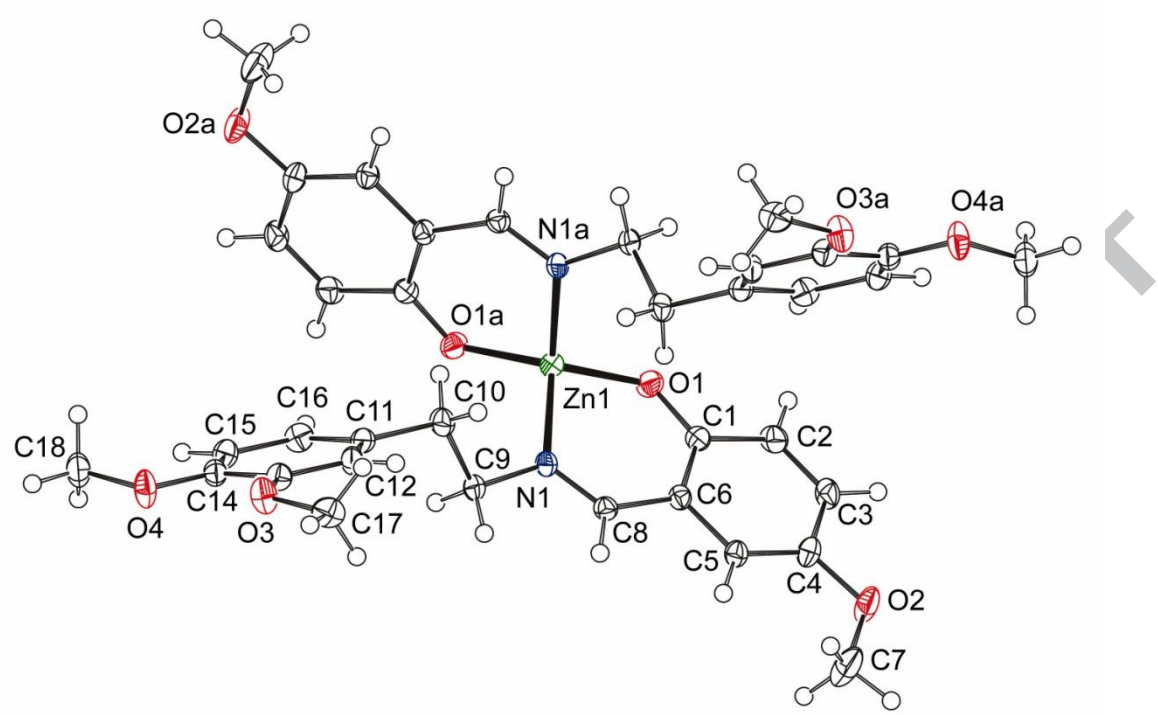

Fig. 2. Structure of the complex **2c** with labeling and thermal ellipsoids drawn at the 50% probability level. Selected bond lengths (Å): Zn(1)–N(1) 2.0005(12), Zn(1)–O(1) 1.9188(10). Selected bond angles (º): O(1)–Zn(1)–N(1) 96.69(4), O(1)–Zn(1)–O(1a) 128.53(7), O(1)–Zn(1)–N(1a) 109.13(5).

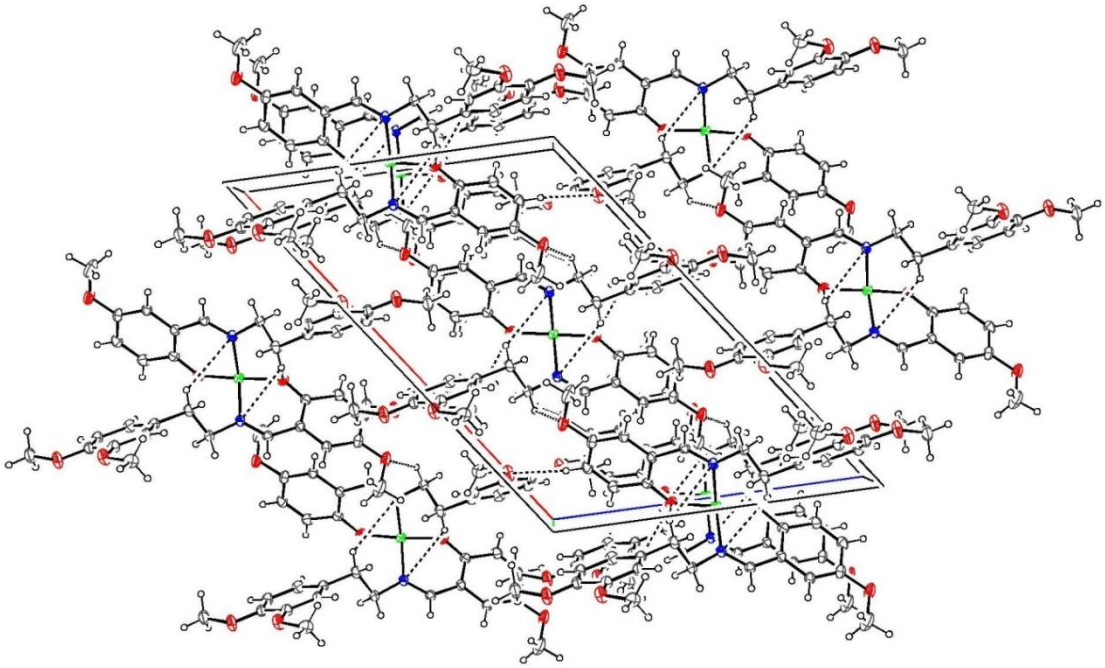

Fig. 3. The crystal packing of **2c**. Dashed lines indicate hydrogen bonds.

The crystal packing of the compound is shown in Fig. 3. In the crystal lattice of **2c** (Fig. 3), all oxygen atoms of each ligand are involved in hydrogen bond interactions. There exists intermolecular hydrogen bonds between the two O(3), O(4) of methoxy groups with H-C(3) of methoxyphenol unit 2.585 Å, 173.03^{o} and 2.747 Å, 118.47^{o}, respectively), intermolecular contacts between O(2) of methoxy group with H-C(9) (2.772 Å, 138.45^{o}) of $(CH_2)_2$ fragments and hydrogen bonding of oxygen atom of phenol unit O(1)···H-C(7) with methoxy group of neighbouring molecules (2.681 Å, 172.39^{o}).

3.4. Electronic absorption spectra and photoluminescence of the zinc complexes

The optical properties of the zinc complexes **2a-d** were investigated by UV-Vis and photoluminescence (PL) spectroscopy in DMSO solutions at room temperature. The results of these studies are summarized in Table 3. The electronic absorption spectra of **2a-d** are shown in Fig. 4.

UV-Vis spectra of the complexes **2a-d** in the spectral range from 300 to 470 nm reveal broad longwave absorption bands with maxima at 354-399 nm (ε = 15260-20890 M^{-1} cm^{-1}). The complex **2d** with the 2-hydroxynaphthaldehyde based ligand additionally has a second higher energy band with λ_{max} = 318 nm (ε = 21530 M^{-1} cm^{-1}) in the same spectral range (Table 3, Fig. 4).

Structural modification of the aldehyde fragment of bidentate azomethine ligands of zinc complexes, associated with the substitution of the 2-tosylamino group (**1a**, λ_{max} = 354 nm) by 2-hydroxy group (**1b**, λ_{max} = 367 nm) leads to an absorption band's bathochromic shift by 13 nm. Additional bathochromic shift ($\Delta\lambda$ = 32 nm) in the absorption spectrum of **1c** (λ_{max} = 399 nm) in comparison with **1b** is achieved due to the introduction of the donor methoxy group into the 2-hydroxybenzylidene fragment.

Table 3

UV-Vis and photoluminescence (PL) data of **2a-d** in DMSO at 293 K: ε – molar extinction coefficient; φ – quantum yield of the fluorescence.

Compound	Absorption λ_{max}, nm (ε, $M^{-1}cm^{-1}$)	Photoluminescence		
		Excitation λ_{max}, nm	Emission λ_{max}, nm	φ
2a	354 (15260) 277 (31500)	352 278	428	0.15
2b	367 (15960) 273 (26100)	366 275	445	0.45
2c	399 (18200) 273sh (27880)	398 275	497	0.11
2d	398 (20890) 318 (21530) 271sh (37550)	397 318 273	443	0.04

sh - Shoulder

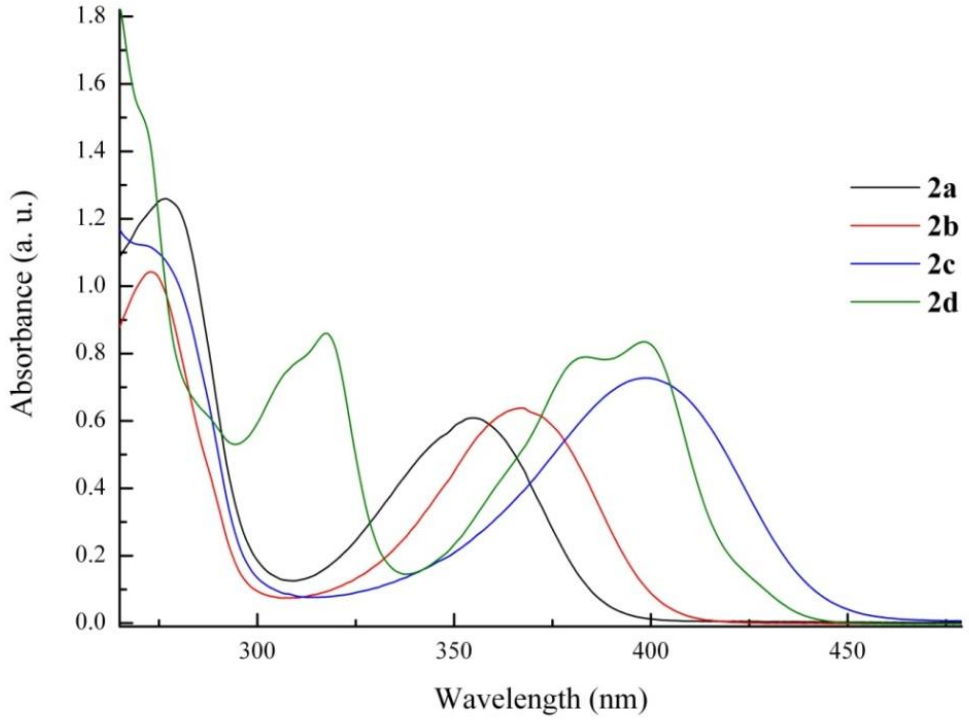

Fig. 4. UV-Vis spectra of compounds **2a-d** in DMSO.

All complexes **2a-d** demonstrate bright blue and green photoluminescence (Table 3, Fig. 5). The fluorescence maxima are located in the wide spectral range of 428 – 497 nm.

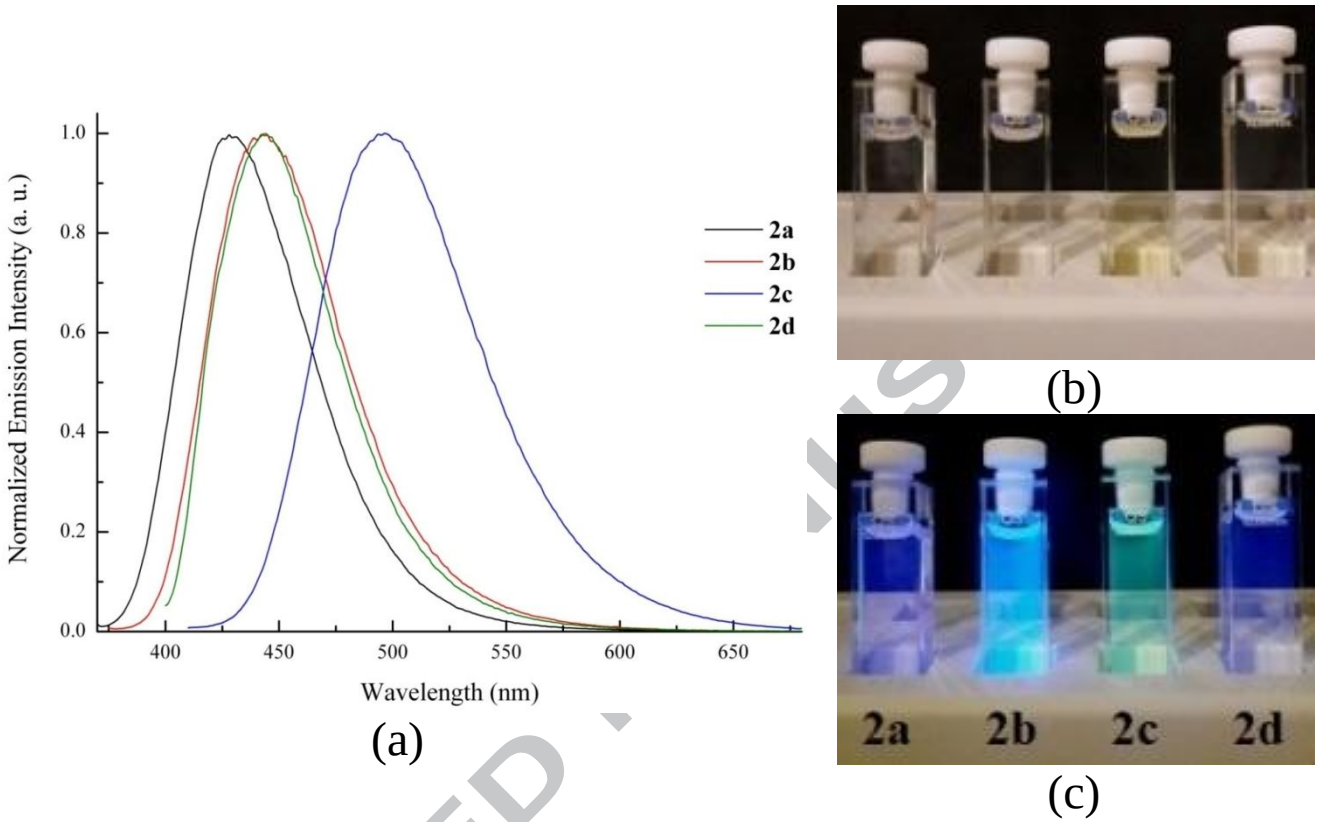

Fig. 5. Normalized emission spectra (λ_{ex} = 365 nm) of compounds **2a-d** in DMSO (a). Solutions photographs of compounds **2a-d** in DMSO: before radiation (no emission) (b); during radiation (photoluminescence, λ_{ex}= 365 nm) at room temperature (c).

In **2a-d** the effect of substituents in the aldehyde fragment of ligands on spectral-fluorescent characteristics is similar to their effect on EAS. The maxima of the emission bands of **2b** (λ_{max} = 445 nm) and **2c** (λ_{max} = 497 nm) are bathochromically shifted by 15-69 nm in comparison with **2a** (λ_{max} = 428 nm).

The fluorescence excitation spectra of **2a–d** fit well their absorption spectra, indicating that their fluorescence was correctly assigned to zinc complexes ZnL_2 (Table 3, Fig. 6).

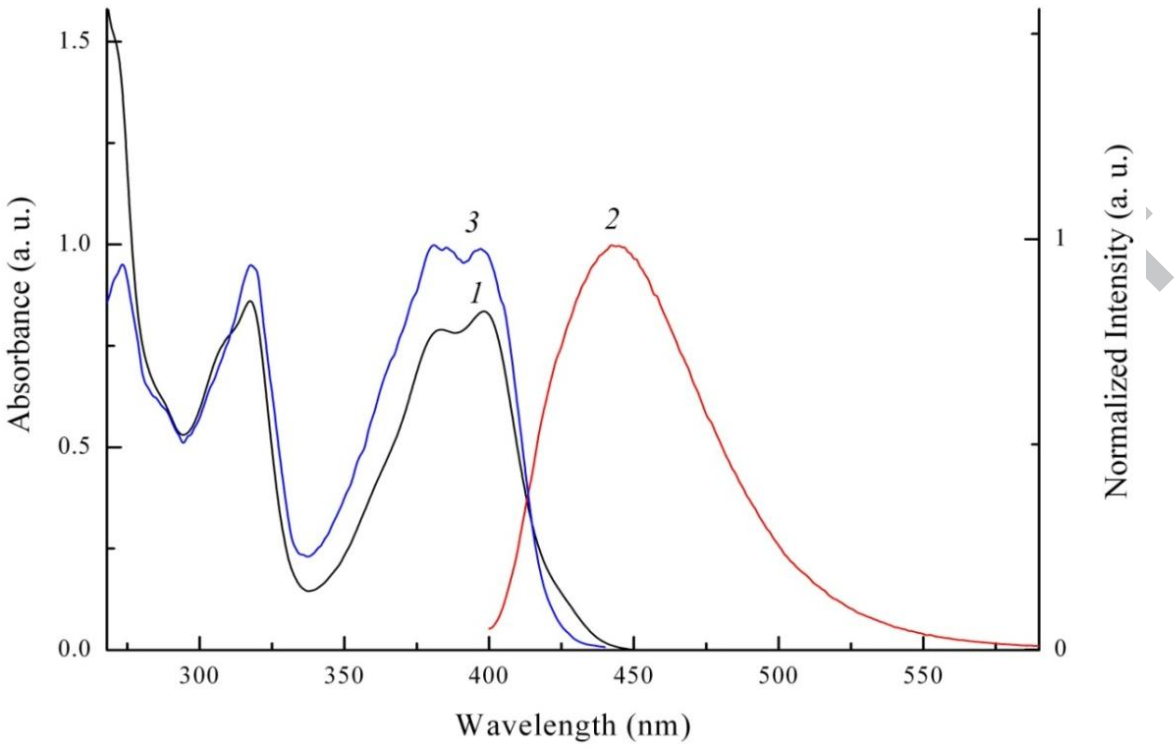

Fig. 6. UV-Vis (*1*), fluorescence emission (λ_{ex} = 400 nm) (*2*) and fluorescence excitation (λ_{obs} = 450 nm) spectra of **2d** in DMSO.

The fluorescence efficiency of the studied compounds also varies over a wide range (φ = 0.04-0.45), depending on their structure (Table 3). Complexes **2a-c** (φ = 0.11-0.45) demonstrate higher quantum yields of fluorescence than their analogue **2d** (φ = 0.04). The introduction of an electron donating 5-methoxy group into the aldehyde fragment leads to a significant quenching of the fluorescence of **2c** (φ = 0.11) in comparison with **2b** (φ = 0.45).

Such spectral characteristics make them promising for use as emitters in the design of light-emitting organic diodes. Earlier, based on zinc complexes with similar ligands, OLED devices were made that demonstrated significant changes in luminescence characteristics depending on the structure of the complex [11, 23, 24, 30]. These devices emitted in the green region of the spectrum with a brightness of 480 to 1470 cd/m^2 (at 12-14 V) and a current density of up to 30 mA/cm^2.

Thus, the above data allows us to conclude that the structural modification of the bidentate azomethine ligands described in this paper (substitution of the N-tosylamino

group by the hydroxy group, introduction of the 5-methoxy group as well as benzannelation) has a significant effect on the optical properties of **2a-d**.

3.5. Interpretation of UV-vis spectra based on TD-DFT calculations

The ground state fully optimized geometry was used to evaluate the excitation energies and oscillator strengths of the electronic excitations of compounds **2a-d** in DMSO solution using TD DFT method. The solvent effect was simulated using the polarizable continuum model (PCM). In Fig. 7, the calculated electronic transitions are characterized by vertical lines with the height proportional to the oscillator strength, the theoretical absorption spectra have been simulated by considering a constant FWHM of 30 nm and compared to the experimental absorption spectra of **2a-d**. The calculated vertical excitation energies, wavelengths, oscillator strengths, and percentage contributions of dominant electronic transitions for complexes **2a-d** are collected in Table 4, along with the experimental transition wavelengths for comparison.

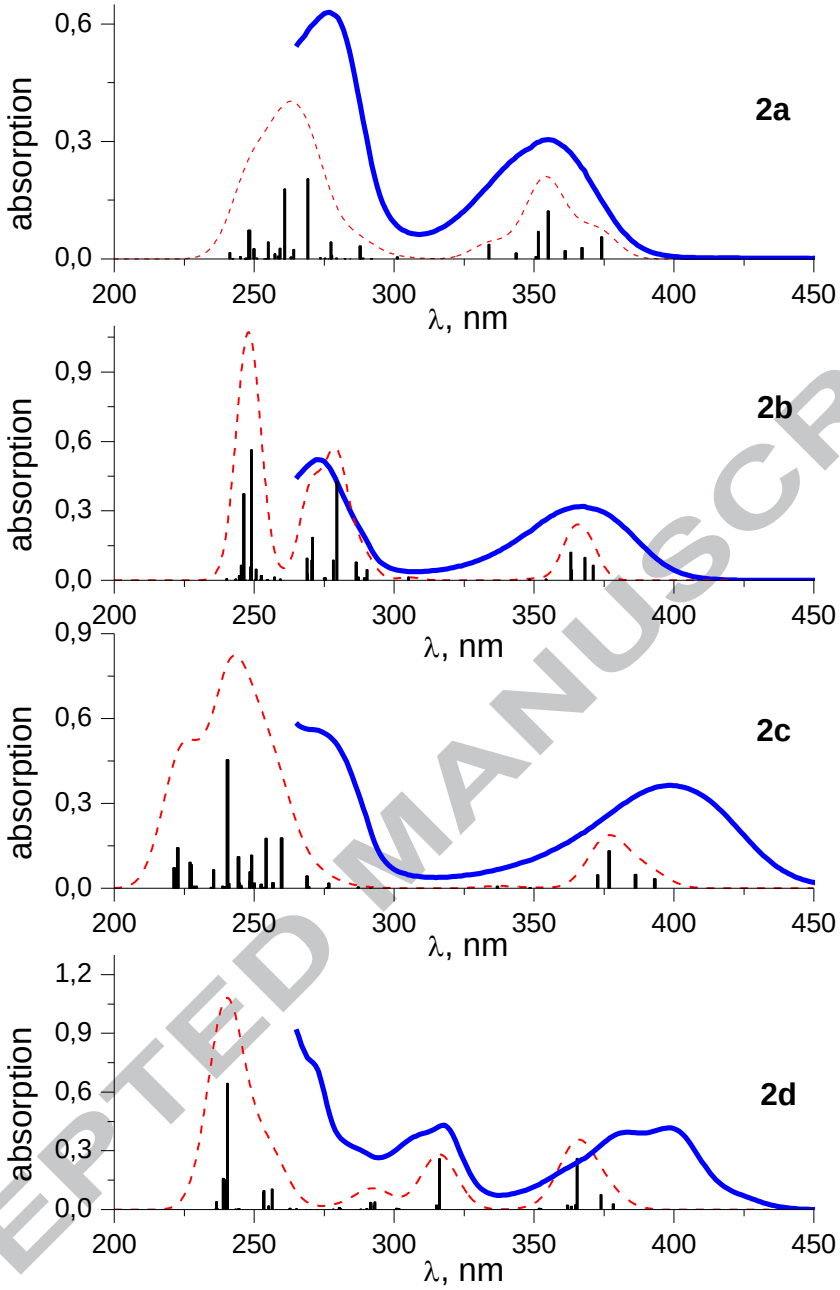

Fig. 7. Comparison of experimental (blue) and TD-DFT calculated (dash red) UV-vis spectra for complexes **2a-d**. Vertical bars represent individual calculated electronic transitions with the height proportional to the oscillator strength.

Table 4

Calculated wavelengths (λ_{max}) and related experimental values (λ_{exp}), energies (E), oscillator strengths (f), involved molecular orbitals and their contributions for different electronic transitions in **2a-d** according to TD-DFT calculations.

complex	λ_{exp}, nm	λ_{max}, nm	E, eV	orbital transition (contribution, %)	f

2a	354	374.18	3.314	HOMO-1 → LUMO (54 %) HOMO-2 → LUMO (26 %)	0.057
		367.14	3.377	HOMO → LUMO (82 %) HOMO-1 → LUMO (16 %)	0.029
		361.15	3.433	HOMO-1 → LUMO (27 %) HOMO-2 → LUMO (61 %)	0.021
		355.12	3.491	HOMO-1 → LUMO+1 (48 %) HOMO-2 → LUMO+1 (25 %)	0.122
2b	367	346.12	3.582	HOMO-1 → LUMO (80 %)	0.064
		343.23	3.612	HOMO → LUMO (85 %)	0.099
		338.47	3.663	HOMO → LUMO+1 (80 %)	0.044
		338.17	3.666	HOMO-1 → LUMO+1 (81 %)	0.120
2c	399	393.13	3.1537	HOMO → LUMO (91 %)	0.034
		386.25	3.2099	HOMO-1 → LUMO(87 %)	0.049
		376.93	3.2893	HOMO → LUMO+1 (83 %)	0.132
		372.78	3.3259	HOMO-1 → LUMO+1 (83 %)	0.047
2d	398 382 318	373.33	3.321	HOMO → LUMO (89 %)	0.028
		368.96	3.360	HOMO-1 → LUMO(82 %)	0.077
		360.42	3.440	HOMO → LUMO+1 (75 %)	0.261
		359.92	3.445	HOMO-2 → LUMO (50 %) HOMO-1 → LUMO+1 (40 %)	0.024
		358.39	3.460	HOMO-3 → LUMO (84 %)	0.017
		356.95	3.473	HOMO-2 → LUMO (39 %) HOMO-1 → LUMO+1 (43 %)	0.023
		311.26	3.983	HOMO-5 → LUMO (59 %) HOMO-4 → LUMO+1 (24 %)	0.260

As can be seen from Fig. 7 the calculated electronic absorption spectra are in good agreement with experiment. This makes it possible to reliably relate the experimental absorption bands to certain electronic transitions forming them.

Analysis of energy characteristics, isosurfaces (Figs. 8-11), and populations (S5-S8 Supplementary Materials) of frontier MOs for **2a-d** demonstrates specific regularities due to the effect of benzaldehyde fragment structural modification of bidentate azomethine ligands. As can be seen from Figs. 8-11 and the data in Table 4, the longwave band in the absorption spectra of zinc complexes **2b-d** is determined, mainly, by $\pi\rightarrow\pi^*$ electronic transitions between quasi-degenerate HOMO and HOMO-1 and LUMO and LUMO+1. The calculation correctly reproduces the experimental bathochromic shift for the **2b-d** complexes, due to the modification of the benzaldehyde fragment of the ligand, which correlates with the energy gap for these complexes. Because of the small difference in the energy values between quasi-degenerate vacant frontier MOs (~ 0.02 eV) for complexes **2a**, **b**, higher electronic transitions with maximal λ_{max} are realized between HOMO-1 $\rightarrow$ LUMO, whereas for complexes **2c**, **d** such are HOMO $\rightarrow$ LUMO. For all **2b-d** complexes the electron density for LUMO and LUMO+1 is localized on both benzaldehyde fragments (Figs. 8-11). The electron density for HOMO and HOMO-1 is localized on both benzaldehyde fragments only for **2c** (Fig. 10), whereas for **2b**,**d** it is delocalized throughout the ligand (excluding zinc ions) (Fig. 9, 11). Thus, in case **2c**, the electronic transitions have the $\pi(L_1)\rightarrow\pi^*(L_1)$ ILCT and $n(O')\rightarrow\pi^*(L_1)$ nature, whereas in **2b**,**d** the transitions have a mixed $\pi(L_2)\rightarrow\pi^*(L_1)$ and $\pi(L_1)\rightarrow\pi^*(L_1)$ LLCT/ILCT type, where O' are atoms of 4-methoxy L_1 benzaldehyde fragments and L_2 is (3,4-dimethoxyphenyl)ethyliminomethyl moiety.

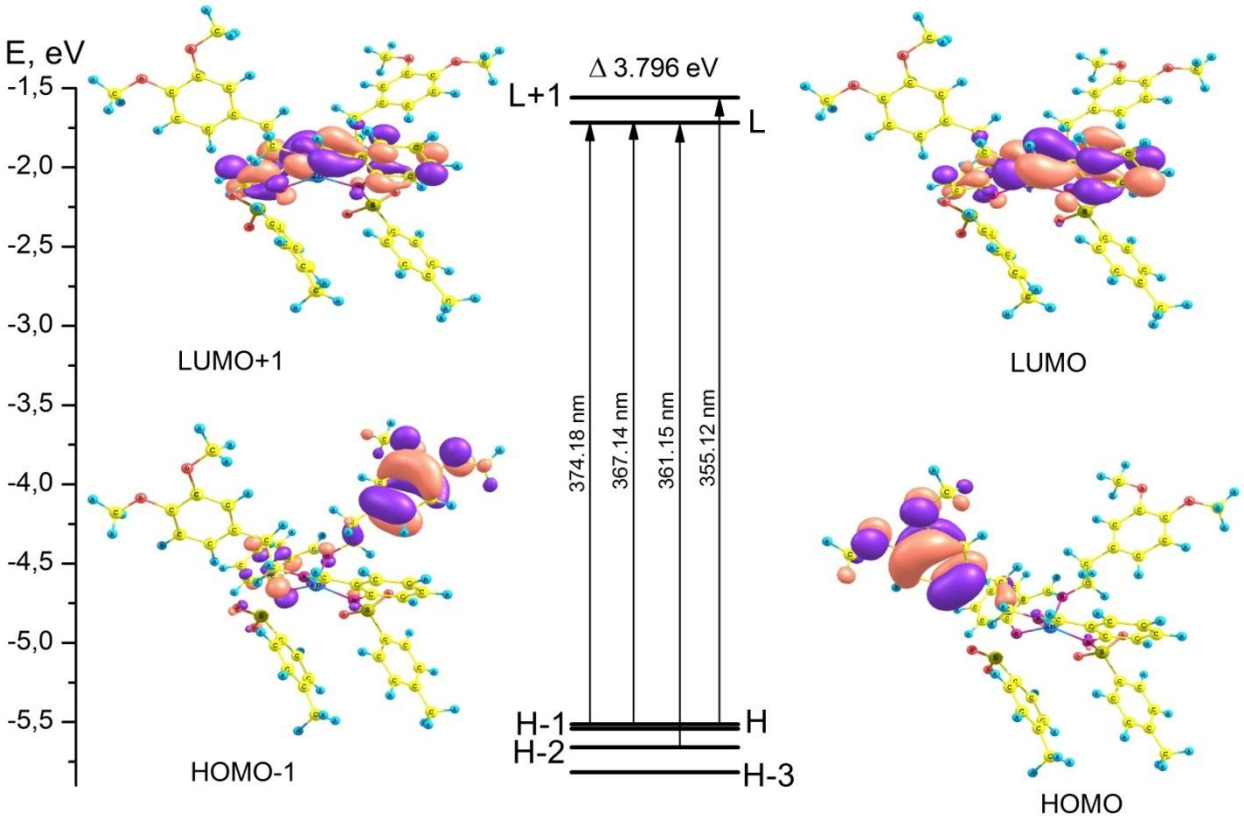

Fig. 8. Molecular orbital energy level diagram for **2a** and contour plots of frontier MOs. The arrows show principal one-electron excitations contributing to the specified low-lying electronic transitions.

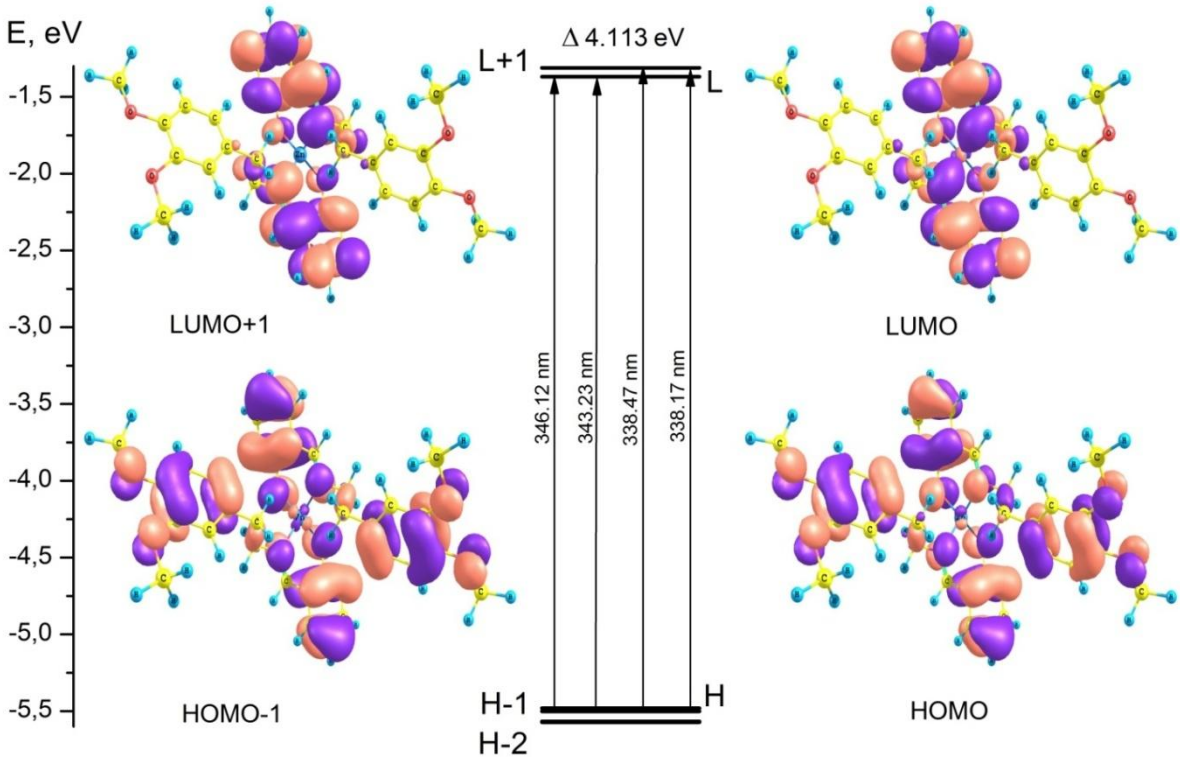

Fig. 9. Molecular orbital energy level diagram for **2b** and contour plots of frontier MOs. The arrows show principal one-electron excitations contributing to the specified low-lying electronic transitions.

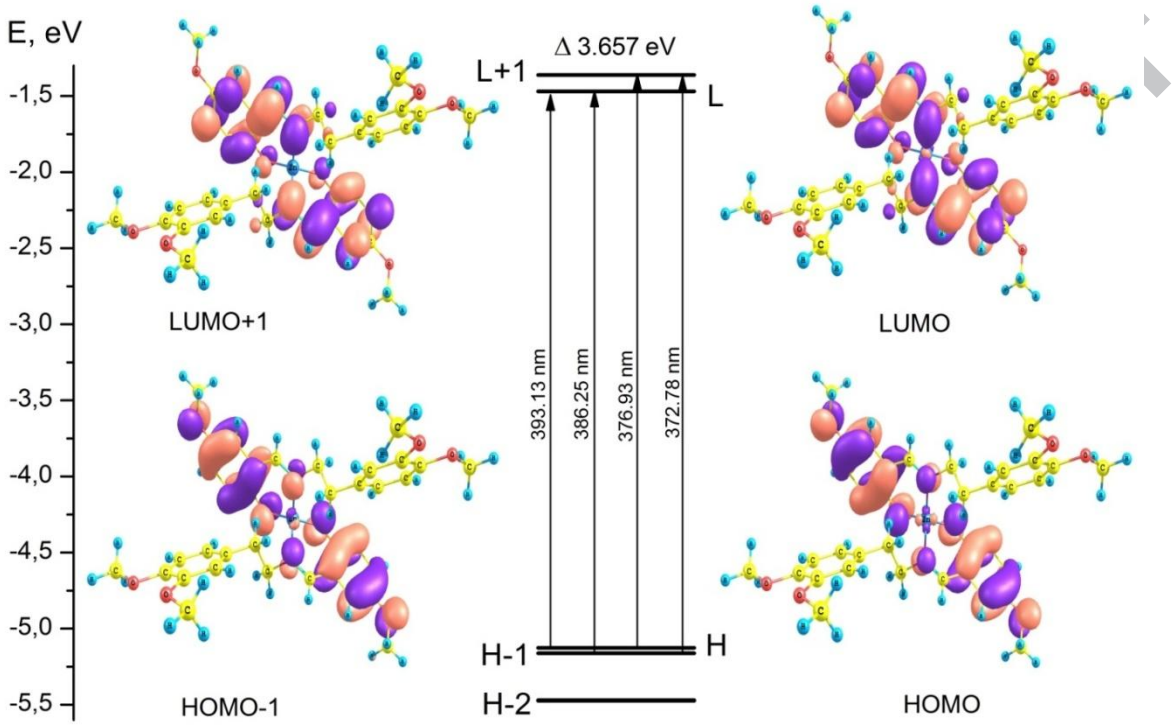

Fig. 10. Molecular orbital energy level diagram for **2c** and contour plots of frontier MOs. The arrows show principal one-electron excitations contributing to the specified low-lying electronic transitions.

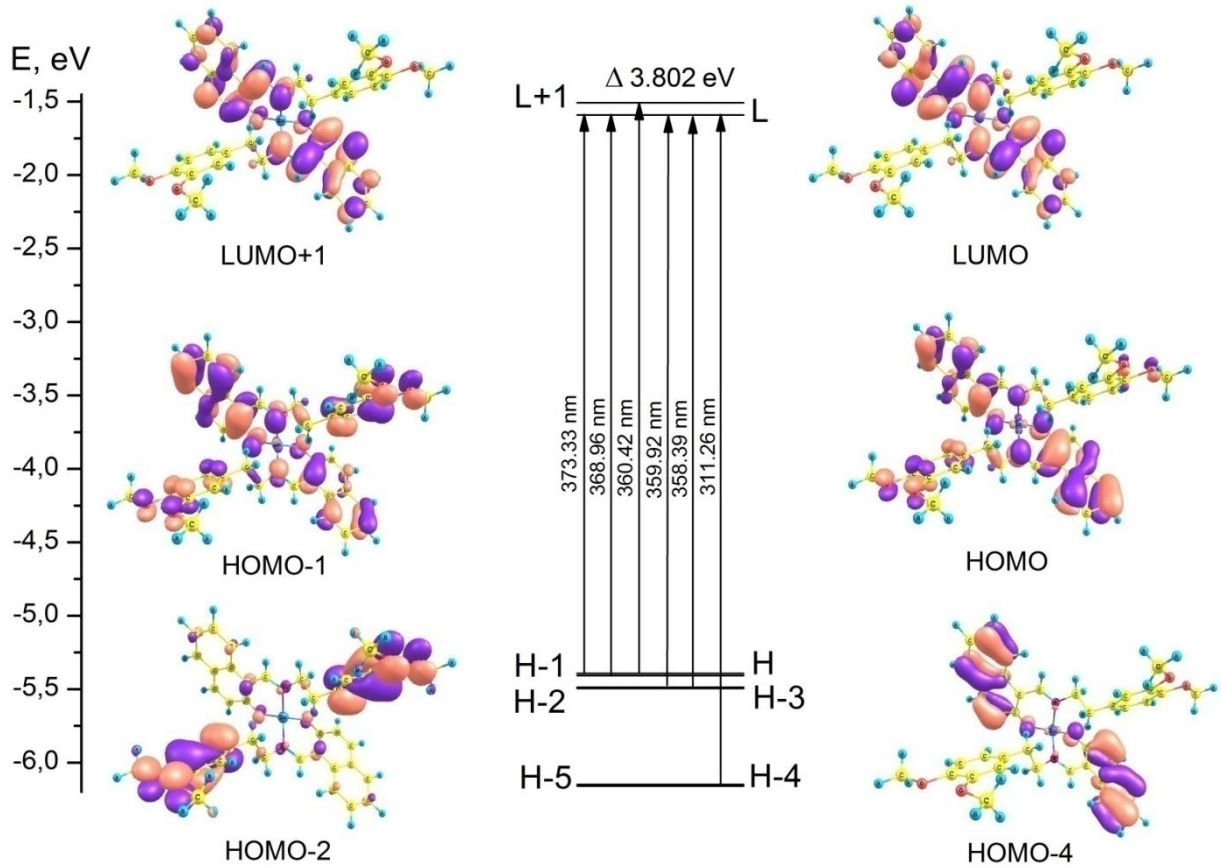

Fig. 11. Molecular orbital energy level diagram for **2d** and contour plots of frontier MOs. The arrows show principal one-electron excitations contributing to the specified low-lying electronic transitions.

The electron absorption band of **2d** at 318 nm, which is absent in spectra of the other complexes **2a-c**, is associated with electronic transitions from HOMO-5 and HOMO-4, whose electron density is localized completely on the naphthalidene-substituted fragment L_1, to LUMO and LUMO+1 and possesses the $\pi(L_1)\rightarrow\pi^*(L_1)$ ILCT character as can be seen from Fig. 11.

In contrast to **2b-d**, the absorption band at 354 nm of **2a** with the N-tosylamine-substituted L_1 fragment is due to the electronic transitions $\pi(L_2)\rightarrow\pi^*(L_1)$ LLCT (Fig. 8).

3.6. Biological activity of the azomethines and zinc complexes

The obtained ligands **1a-d** and zinc complexes **2a-d** were investigated for antibacterial, protistocidal and fungistatic activity and the results are summarized in Table 5.

Table 5

Fungistatic, protistocidal and bacteriostatic activity of ligands **1a-d** and zinc complexes **2a-d**.

Compound	*Penicillium italicum*, inhibition zone diameter (mm)	*Colpoda steinii* (μg/mL)	*Escherichia coli 078* (μg/mL)	*Staphylococcus aureus P-209* (μg/mL)
1a	0	62.5	>500	>500
1b	0	250	>500	>500
1c	6	250	>500	>500
1d	6	125	>500	>500
2a	8.0	>500	>500	>500
2b	10.0	>500	>500	>500
2c	8.0	>500	>500	>500
2d	8.0	>500	>500	>500
Sulfadimethoxine	-	-	62.5	62.5
Toltrazuril	-	62.5	-	-
Fundazol	22	-	-	-

It can be found from the data in Table 5 that ligands **1a-d** and complexes **2a-d** do not have bacteriostatic activity against *Escherichia coli*, *Staphylococcus aureus*. The most important result was obtained in the study of protistocidal and fungistatic properties. Ligands **1a-d** show high protistocidal activity: the compound **1a** has the same activity as toltrazuril, whereas the ligand **1d** is twice less active, and azomethines **1b**,**c** are four times less active. Azomethines **1a-d** show similar or lower protistocidal activity comparing to their analogues containing a hydroxyalkyliminomethyl group instead of the 2-(3,4-dimethoxyphenyl)ethyliminomethyl group [12].

Unlike ligands **1a-d**, the complexes **2** do not possess protistocidal activity against *Colpoda steinii*. Some ligands and complexes have fungistatic activity, but they are less active against *Penicillium italicum* than fundazol (ligands **1c**,**d** - four times, complexes

2a,**c**,**d** - three times, and complex **2b** - two times less active). Complexes **2a-d** have the same fungistatic activity values as their analogues containing a hydroxyalkyliminomethyl group instead of 2-(3,4-dimethoxyphenyl)ethyliminomethyl group [12].

Thus, some representatives of zinc complexes **2** show higher fungistatic activity in comparison with ligands, whereas two complexes exhibit fungistatic activity that is not observed in the corresponding ligands, and in two complexes fungistatic activity increased 1.3 times with respect to the activity of the corresponding ligands. Unlike the complexes, ligands show high protistocidal activity: one compound has the same activity as toltrazuril, and the other is two times less active. Therefore, it may be concluded that the search for antiprotozoal drugs in the azomethine series containing 2-(3,4-dimethoxyphenyl)ethyliminomethyl group in the phenyl or naphthalene ring is promising, whereas the zinc complexes with these ligands can be perspective for fungicidal drug design.

Conclusion

Four new azomethine compounds of the derivatives of 2-tosylamino, 2-hydroxybenzaldehydes, 2-hydroxynaphthaldehyde, and 3,4-dimethoxyphenylethylamine were synthesized. Zinc complexes were obtained on their basis by chemical and electrochemical methods. The local atomic structure of the complexes was determined by X-ray absorption spectroscopy. The crystal and molecular structure of bis{2-[(E)-2-(3,4-dimethoxyphenyl)ethyliminomethyl]-4-methoxyphenol}zinc(II) was determined by the X-ray diffraction method. The spectral characteristics of zinc complexes were investigated. The bands of electronic absorption spectra of the complexes were interpreted using the results of quantum chemical calculations in the TD-DFT approximation.

Zinc complexes (ZnL_2) are thermally stable with m.p. in the range 194 - 248 ^{o}C and exhibit efficient photoluminescent properties in the blue spectral region from 428 to 497 nm. Such spectral characteristics make them promising for use as emitters in the

design of light-emitting organic diodes. The antibacterial, protistocidal, and fungistatic activities of the obtained azomethines and their zinc complexes were studied.

Acknowledgements

The work was performed with the financial support of the Ministry of Education and Science of the Russian Federation (the State assignment: project 4.5388.2017/8.9). IR, NMR, UV-Vis and PL spectra were obtained using facilities of the "Molecular Spectroscopy" Multi-user Center of the Southern Federal University. X-ray absorption spectra were measured at the Unique Scientific Facility Kurchatov Synchrotron Radiation Source funded by the Ministry of education and science of the Russian Federation (project RFMEFI61914X0002).

References

[1] Z.H. Chohan, M. Arif, N. Sarfraz, Appl. Organomet. Chem. 21 (2007) 294.

[2] M.T. Kaczmarek, R. Jastrza, E. Holderna-Kedzia, V. Radetzky-Paryzek, Inorg. Chim. Acta. 362 (2009) 3127.

[3] Q. Huang, Z.Q. Pan, P. Wang, Z.P. Chen, X.L. Zhang, H.S. Xu, Bioorg. Med. Chem. Lett. 16 (2006) 3030.

[4] M.C. Rodrìguez-Argüelles, M. Ferrari Belichi, F. Bisceglie, C. Pelizzi, G. Pelosi, S. Pinelli, M. Sassi, J. Inorg. Biochem. 98 (2004) 313.

[5] H. Zhang, C.S. Liu, X.H. Bu, M. Yang, J. Inorg. Biochem. 99 (2005) 1119.

[6] Z. Trávníček, V. Kryštof, M. Šipl, J. Inorg. Biochem. 100 (2006) 214.

[7] X. Sheng, X. Guo, M.X. Lu, Y.G. Lu, Y. Shao, F. Liu, Bioconjugate Chem. 19 (2008) 490.

[8] J.Tang, B.Wang, L. Zhu, Bioorg. Med. Chem. 17 (2009) 614.

[9] Q. Jiang, J. Zhu, Y. Zhang, N. Xiao, Z. Guo, Biometal. 22 (2009) 297.

[10] A.P. Pushkarev, M.N. Bochkarev, Russ. Chem. Rev.85 (2016) 1338.

[11] A.S. Burlov, V.G. Vlasenko, D.A. Garnovskii, A.I. Uraev, E.I. Mal'tsev, D.A. Lypenko, A.V. Vannikov. Electroluminescent organic light-emitting diodes based on coordination compounds. Rostov-on-Don: S.F.U., 2015. 228 p.

[12] A.S. Burlov, V.G. Vlasenko, Yu.V. Koshchienko, N.I. Makarova, A.A. Zubenko, Yu.D. Drobin, G.S. Borodkin, A.V. Metelitsa, Ya.V. Zubavichus, D.A. Garnovskii, Polyhedron 144 (2018) 249.

[13] A.S. Burlov, Yu.V. Koshchienko, N.I.Makarova, T.A. Kuz'menko, V.V. Chesnokov, M.A. Kiskin, S.A. Nikolaevskii, D.A. Garnovskii, A.I. Uraev, V.G. Vlasenko, A.V. Metelitsa, Synth. Met. 220 (2016) 543.

[14] A.S. Burlov, V.G. Vlasenko, A.V. Dmitriev, V.V. Chesnokov, A.I. Uraev, D.A. Garnovskii, Y.V. Zubavichus, A.L. Trigub, I.S. Vasilchenko, D.A. Lypenko, E.I. Mal’tsev, T.V. Lifintseva, G.S. Borodkin, Synth. Met. 203 (2015) 156.

[15] A.V. Metelitsa, A.S. Burlov, S.O. Bezugly, I.G. Borodkina, V.A. Bren, A.D. Garnovskii, V.I. Minkin, Russ. J. Coord. Chem. 32 (2006) 858.

[16] A.S. Burlov, E.I. Mal'tsev, V.G. Vlasenko, D.A. Garnovskii, A.V. Dmitriev, D.A. Lypenko, A.V. Vannikov, P.V. Dorovatovskii, V.A. Lazarenko, Y.V.Zubavichus, V.N. Khrustalev, Polyhedron 133 (2017) 231.

[17] A.S. Burlov, V.G. Vlasenko, N.I. Makarova, K.A. Lysenko, V.V. Chesnokov, G.S. Borodkin, I.S. Vasilchenko, A.I. Uraev, A.D.Garnovskii, A.V. Metelitsa, Polyhedron. 107 (2016) 153.

[18] U. Caruso, B. Panunzi, A. Roviello, A. Tuzi, Inorg. Chem. Comm. 29 (2013) 138.

[19] M. Argeri, F. Borbone, U. Caruso, M. Causà, S. Fusco, B. Panunzi, A. Roviello, R. Shikler, A. Tuzi, Europ. J. Inorg. Chem. 34 (2014) 5916.

[20] F. Borbone, U. Caruso, S. Concilio, S. Nabha, B. Panunzi, S. Piotto, R. Shikler, A. Tuzi, Europ. J. Inorg. Chem. 6 (2016) 818.

[21] T. Sano, Y. Nishio, Y. Hamada, H. Takahashi, T. Usuki, K. Shibata, J. Mater. Chem. 10 (2000) 157.

[22] L. Chen, J. Qiao, J. Xie, L. Duan, D. Zhang, L. Wang, Y. Qiu, L. Chen, Inorg. Chim. Acta. 362 (2009) 2327.

[23] A.P. Pivovarov, M.G. Kaplunov, I.K. Yakushchenko, M.Yu. Belov, G.V. Nikolaeva, O.N. Efimov, Russ. Chem. Bull. 51 (2002) 67.

[24] M.G. Kaplunov, I.K. Yakushchenko, S.S. Krasnikova, S.N. Shamaev, A.P. Pivovarov, O.N. Efimov, Russ. Chem. Bull. 53 (2004) 2148.

[25] M.R. Bormejo, M. Vazques, J. Sanmartín, A.M. García-Deibe, M. Fondo, C. Lodeiro, New Journ. Chem. 26 (2002) 1365.

[26] A.V. Metelitsa, A.S. Burlov, S.O. Bezuglyi, I.G. Borodkina, V.A. Bren, A.D. Garnovskii, V.I. Minkin, Russ. J. Coord. Chem. 32 (2006) 858.

[27] A.S. Burlov, D.A. Garnovskii, L.I. Kuznetsova, N.V. Volbushko, O.Yu. Korshunov, O.T. Asmaev, B.I. Kharisov, L.M. Blanco, A.D. Garnovskii, Russ. J. Coord. Chem. 24 (1998) 857.

[28] A.D. Garnovskii, A.S. Burlov, A.V. Metelitsa, I.G. Borodkina, K.A. Lysenko, S.O. Bezuglyi, E.D. Garnovskaya, E.V. Sennikova, G.S. Borodkin, D.A. Garnovskii, Russ. J. Gen. Chem. (2010) 80(2) 292.

[29] A.S. Burlov, V.V. Chesnokov, V.G. Vlasenko, D.A. Garnovskii, E.I. Mal'tsev, A.V. Dmitriev, D.A. Lypenko, G.S. Borodkin, Yu.V. Revinskii, Russ. Chem ll. 63 (2014) 1753.. Bu

[30] A.S. Burlov, E.I. Mal'tsev, V.G. Vlasenko, A.V. Dmitriev, D.A. Lypenko, D.A. Garnovskii, A.I. Uraev, G.S. Borodkin, A.V. Metelitsa, Russ. Chem. Bull. 63 (2014) 1759.

[31] N.I. Chernova, Y.S. Ryabokobylko, V.G. Brudz, B.M. Bolotin, Zh. Org. Khim. 7 (1971) 1680.

[32] S. Parker, Photoluminescence of Solutions, Mir, Moskow (1972), 247 p.

[33] B. M. Krasovitskii, B.M. Bolotin, Organic Luminophores [in Russian], Khimiya, Moscow, 1984, p. 292.

[34] G.M. Sheldrick, SHELXL97. Program for the Refinement of Crystal Structures. University of G6ttingen, Germany (1997).

[35] A.A. Chernyshov, A.A. Veligzhanin, Y.V. Zubavichus, Nucl. Instr. Meth. Phys. Res. A. 603 (2009) 95.

[36] B. Ravel and M. Newville, J. Synchr. Rad. 12 (2005) 537.

[37] S.I. Zabinski, J.J. Rehr, A. Ankudinov, R.C. Albers, M. Eller, J. Phys. Rev. B. 52 (1995) 2995.

[38] M.J. Frisch, G.W. Trucks, H.B. Schlegel, G.E. Scuseria, M.A. Robb, J.R. Cheeseman, J.A. Montgomery, Jr. T. Vreven, K.N. Kudin, J.C. Burant, J.M. Millam, S.S. Iyengar, J. Tomasi, V. Barone, B. Mennucci, M. Cossi, G. Scalmani, N. Rega, G.A. Petersson, H. Nakatsuji, M. Hada, M. Ehara, K. Toyota, R. Fukuda, J. Hasegawa, M. Ishida, T. Nakajima, Y. Honda, O. Kitao, H. Nakai, M. Klene, X. Li, J.E. Knox, H.P. Hratchian, J.B. Cross, V. Bakken, C. Adamo, J. Jaramillo, R. Gomperts, R.E. Stratmann, O. Yazyev, A.J. Austin, R. Cammi, C. Pomelli, J.W. Ochterski, P.Y. Ayala, K. Morokuma, G.A. Voth, P. Salvador, J.J. Dannenberg, V.G. Zakrzewski, S. Dapprich, A.D. Daniels, M.C. Strain, O. Farkas, D.K. Malick, A.D. Rabuck, K. Raghavachari, J.B. Foresman, J.V. Ortiz, Q. Cui Piskorz, I. Komaromi, R.L. Martin, D.J. Fox, T. Keith, M.A. Al-Laham, C.Y. Peng, A. Nanayakkara, M. Challacombe, P.M.W. Gill, B.

Johnson, W. Chen, M.W. Wong, C. Gonzalez, J.A. Pople,Gaussian 03, Revision A.1, Gaussian, Inc., Pittsburgh PA, USA (2003).

[39] A.D. Becke, J. Chem. Phys. 98 (1993) 5648.

[40] C. Lee, W. Yang, R.G. Parr, Phys. Rev. 37 (1988) 785.

[41] G.A. Petersson, A. Bennett, T.G. Tensfeldt, M.A. Allaham, W.A. Shirley, J. Mantzaris, J. Chem. Phys. 89 (1988) 2193.

[42] R. Ditchfield, W.J. Hehre, J.A. Pople, J. Chem. Phys. 54 (1971) 724.

[43] J. Tomasi, B. Mennucci, R. Cammi, Chem. Rev. 105 (2005) 2999.

[44] Determination of the Sensitivity of Microorganisms to Antibacterial Drugs: Guidelines. MUK 4.2.1890-04, Moscow: Medicine, 2004.

[45] G.N. Pershin, Methods of Experimental Chemotherapy, Moscow: Medicine, 1971, p. 100.

[46] L.N. Fetisov, A.A. Zubenko, A.N. Bodryakov, M.A. Bodryakova, Proc. Int. Parasitol. Symp."Modern Problems of General and Partial Parasitology" (2012) 70.

[47] Manual on Experimental (Preclinical) Study of New Pharmaceuticals, Khabriev, R.U. (Ed.), Moscow: Medicine, 2005.

[48] A.S. Burlov, V.G. Vlasenko, D.A. Garnovskii, N.V. Polosareva, A.S. Antsyshkina, G.G. Sadikov, V.S. Sergienko, A.V. Churakov, Y.V. Zubavichus, E.I. Mal'Tsev, A.V. Dmitriev, D.A. Lypenko, A.S. Cheprasov, G.S. Borodkin, A.V. Metelitsa, Russ. J. Inorg. Chem. 59(7) (2014) 721.

[49] A.S. Burlov, S.A. Mashchenko, V.G. Vlasenko, Y.V. Zubavichus, A.I. Uraev, K.A. Lyssenko, S.I. Levchenkov, I.S. Vasilchenko, D.A. Garnovskii, G.S. Borodkin, Journ. Mol. Stuct., 1061 (2014) 47.

[50] Y.V. Koshchienko, A.S. Burlov, N.I. Makarova, V.G. Vlasenko, S.A. Nikolaevskii, M.A. Kiskin, D.A Garnovskii, A.L. Trigub, A.V. Metelitsa, |Russ. J. Gen. Chem. 87(4) (2017) 764.

Graphical Abstract

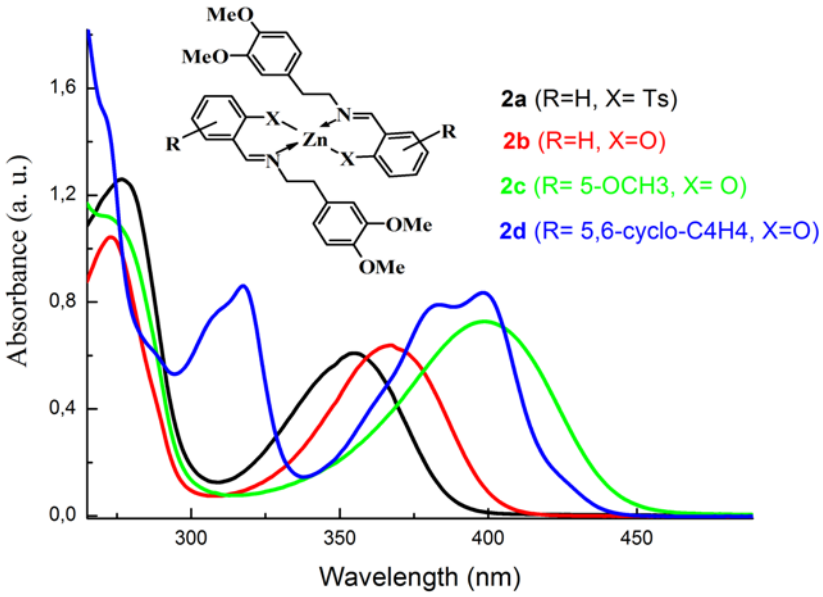

Synopsis

The complexes of zinc(II) with a bidentate azomethine Schiff base ligands derived from 2-tosylaminobenzaldehyde, 2-hydroxy-5-methoxybenzaldehydes, 2-hydroxynaphthaldehyde and 3,4-dimethoxyphenylethylamine were synthesized and characterized. The azomethines and complexes of zinc have been screened for their antibacterial, protistocidal, and fungistatic activities.